

Variational Sampling of Temporal Trajectories

Jurijs Nazarovs¹, Zhichun Huang², Xingjian Zhen¹, Sourav Pal¹, Rudrasis Chakraborty³, Vikas Singh¹

¹University of Wisconsin-Madison

²Carnegie Mellon University

³Butlr

nazarovs@wisc.edu, zhichunh@alumni.cmu.edu, zhenxingjian1995@gmail.com, spal9@wisc.edu,

rudrasischa@gmail.com, vsingh@biostat.wisc.edu

https://github.com/vsingh-group/functional_node

Abstract

A deterministic temporal process can be determined by its trajectory, an element in the product space of (a) initial condition $z_0 \in \mathcal{Z}$ and (b) transition function $f : (\mathcal{Z}, \mathcal{T}) \rightarrow \mathcal{Z}$ often influenced by the control of the underlying dynamical system. Existing methods often model the transition function as a differential equation or as a recurrent neural network. Despite their effectiveness in predicting future measurements, few results have successfully established a method for sampling and statistical inference of trajectories using neural networks, partially due to constraints in the parameterization. In this work, we introduce a mechanism to learn the distribution of trajectories by parameterizing the transition function f explicitly as an element in a function space. Our framework allows efficient synthesis of novel trajectories, while also directly providing a convenient tool for inference, i.e., uncertainty estimation, likelihood evaluations and out-of-distribution detection for abnormal trajectories. These capabilities can have implications for various downstream tasks, e.g., simulation and evaluation for reinforcement learning.

1 Introduction

Learning to predict and infer from temporal/sequential data is an important topic in machine learning, with numerous application in many settings, including semantic video processing (Nilsson and Sminchisescu 2018) in vision and text generation/completion (Lewis et al. 2019; Radford et al. 2018) in natural language processing. The literature has continued to evolve, from handling evenly-sampled discrete observations (e.g., LSTM (Hochreiter and Schmidhuber 1997), GRU (Cho et al. 2014)) to irregularly-sampled or even continuous observations (e.g., Neural ODE (Chen et al. 2018) / SDE (Rubanova, Chen, and Duvenaud 2019; Tzen and Raginsky 2019)). These capabilities have been extensively used, from learning complex non-linear tasks such as language modeling (Devlin et al. 2018) to forecasting of physical dynamics (Lusch, Kutz, and Brunton 2018; Brunton, Noack, and Koumoutsakos 2020; Rudy et al. 2017).

Despite the mature state of various methods currently available for prediction tasks involving temporal sequences, fewer options exist that allow sampling from distribution of trajectories, similar to VAE for standard images, and can provide the confidence of their predictions. Existing methods, such as

Neural ODEs, do facilitate the ability to sample trajectories by varying the initial conditions of the underlying differential equation. However, these methods are limited in their ability to model real-world systems where the *same* initial conditions can result in vastly different outcomes, (e.g. common in reinforcement learning). Also, brain development of identical twins can differ despite starting from exactly the same state (Strike et al. 2022). To address this limitation, Bayesian versions of Neural ODEs, similar to stochastic differential equations, can account for uncertainty in trajectories. However, these methods are not designed to handle a wide variety of different trajectories with the same initial point and primarily not used as methods to sample dynamical processes. How can we address the problem of sampling a wide variety of different trajectories with the same initial condition? In other words, given an NODE setup in (1), where f is NN, can we learn a mechanism, which allows us to sample f as an element from a functional space of NN?

At a high level, one inspiration of our work is a recent result dealing with explicit embeddings of neural network functions (Dupont et al. 2022). We can treat the transition function f of the trajectory as an entity on its own and embed it explicitly in a Euclidean space. There, we can conveniently learn the distribution of embeddings which in-turn can help us learn the distribution of the trajectories. Then, we can directly estimate the likelihoods and even sample new trajectories, with little to no overhead. Ideally, the embedding space will also have far fewer dimensions compared to the dimension of the data, which can make the distribution easier to learn. While Dupont et al. (2022) have explored learning the distribution of data-generating neural network functions through explicit embeddings termed *functas*, our work extends such an idea to infer temporal trajectories by jointly constructing an appropriate functional embedding space for trajectories and learning a variational statistical model on top.

Contributions: We study a simple mechanism to embed the trajectory of temporal processes and show that one can directly perform variational inference of trajectories in this embedding space. The end result is a probabilistic model that allows efficient sampling and likelihood estimation of novel trajectories, which is immediately useful for simulation and for applications that require statistical inference,

such as outlier detection. We show via experiments that the proposed framework can achieve competitive performance in prediction tasks compared with conventional temporal models, while benefiting from the additional capabilities described above, already baked into the formulation.

2 Background/notation

Notation: We denote a time-varying vector with T time steps as $\mathbf{z} = (\mathbf{z}_0, \dots, \mathbf{z}_{T-1})$, where each time step \mathbf{z}_t is a vector valued sample, specifically $\mathbf{z}_t \in \mathbf{R}^p$, where p is the number of covariates/channels.

(Neural) Ordinary Differential Equations: We consider the ODE as $\dot{\mathbf{z}}_t = f(\mathbf{z}_t, t)$ to model transitions, where $f(\mathbf{z}_t, t)$ represents a change in state \mathbf{z}_t at time step t , and depends on a value of a state of the process at time t . Given the initial time t_0 and target time t , ODEs compute the corresponding state \mathbf{z}_t by performing the following operations:

$$\mathbf{z}(t_0) = \mathbf{z}_0, \quad \mathbf{z}(t) = \mathbf{z}(t_0) + \int_{t_0}^t f(\mathbf{z}_t, t) dt \quad (1)$$

Parameterized neural networks have been shown to model $f(\mathbf{z}_t, t)$ for complex nonlinear dynamics as in (Chen et al. 2018; Kidger et al. 2020).

Learning latent representations with a VAE: One of our goals is to learn a latent representation of a temporal trajectory, and so we focus on variational approximation techniques. Recall that Variational auto-encoders (VAE) (Kingma and Welling 2013) learn a probability distribution on a latent space. We can draw samples in the latent space and the decoder can generate samples in the space of observations. In practice, the parameters of the latent distribution are learned by maximizing the *evidence lower bound* (ELBO) of the intractable likelihood:

$$\log p(\mathbf{x}) \geq -KL(q(\mathbf{z})\|p(\mathbf{z})) + \mathbb{E}_{q(\mathbf{z})} [\log p(\mathbf{x}|\mathbf{z})] \quad (2)$$

where \mathbf{z} is a sample in the latent space from the approximate posterior distribution $q(\mathbf{z})$, with a prior $p(\mathbf{z})$, and \mathbf{x} is a reconstruction of a sample (e.g., an image or temporal sample) with the likelihood $p(\mathbf{x}|\mathbf{z})$. One choice for q is $\mathcal{N}(\mu, \Sigma)$, where μ and Σ are trainable parameters (Kingma and Welling 2013). Note, $\mathbf{z} \in \mathcal{Z}$ denotes a latent space sample and $\mathbf{x} \in \mathcal{X}$ denote an observed space sample.

3 Variational Sampling of Temporal Trajectories

We start with deterministic temporal processes which can be defined by the corresponding trajectory on the underlying space \mathcal{Z} . A trajectory can be identified by an element in the product space of (a) initial condition $\mathbf{z}_0 \in \mathcal{Z}$ (often given) and (b) transition function $f : \mathcal{Z} \times [0, T] \rightarrow \mathcal{Z}$ often influenced by the control of the underlying dynamical system. Thus, to learn the distribution of the temporal process, it is necessary to learn distributions over both the initial condition \mathbf{z}_0 and the transition function f .

One way to model transition function between states \mathbf{z}_t of the temporal process is by using the ODE: $\dot{\mathbf{z}}_t = f(\mathbf{z}_t, t)$. We know that one can parameterize $f(\mathbf{z}_t, t)$ by a neural network (NN) $f_\theta(\mathbf{z}_t, t)$ to leverage their function approximation

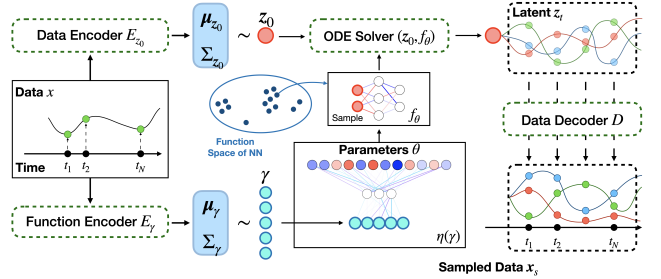


Figure 1: Structure of the model. First, Data Encoder is applied to temporal data sample to generate the initial point of the trajectory in latent space \mathbf{z}_0 ; At the same time, the Function Encoder (embedding module) is applied to generate parameterization θ of the sample from function space, f_θ . The sample from function or embedding space, f_θ , is used to describe together with a differential equation solver, to solve function DE and generate \mathbf{z}_t . Last, decoder is used to map latent space ODE stages into observed values.

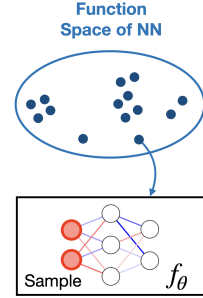


Figure 2: Function/embedding space, where each element is a DNN.

capacity (Chen et al. 2018). Thus, we can (possibly) use a NN to describe a trajectory. However, if we want to sample from this space of trajectories using the above NN parameterization, we must learn a latent representation of a NN, analogous to INR (Dupont et al. 2022).

3.1 Functional Neural ODE

Goal: Given a dataset of N temporal observations with length T , $\{\mathbf{x}^{(i)}\}_{i \in [N]} = \{\mathbf{x}_0^{(i)}, \dots, \mathbf{x}_{T-1}^{(i)}\}_{i \in [N]}$, we seek to learn a set of parameters $(\phi_E, \phi_D, \phi_\gamma)$ corresponding to data encoder/decoder (E_{z0}, D) and function encoder E_γ (as shown in Figure 2) such that $p(\mathbf{x}^{(i)})$ is maximized. Formally, we can solve the following problem

$$\max \frac{1}{N} \sum_{i=1}^N p(\mathbf{x}^{(i)}) \equiv \max_{\phi_D} \frac{1}{N} \sum_{i=1}^N p_{\phi_D}(\mathbf{x}^{(i)} | \mathbf{z}_0, f_\theta) p(\mathbf{z}_0, \theta) \quad (3)$$

where \mathbf{z}_0 is the initial condition, and f_θ is a NN with weights θ inferred from the data. Similar to VAE, since we do not know the true posterior distribution $p(\mathbf{z}_0, \theta)$, we replace it with a variational distribution $p(\mathbf{z}_0, \theta) \approx q_{\phi_E}(\mathbf{z}_0 | \mathbf{x}^{(i)}) q_{\phi_\gamma}(\theta | \mathbf{x}^{(i)})$. The resultant objective is

$$\max_{\phi_E, \phi_D, \phi_\gamma} \frac{1}{N} \sum_{i=1}^N p_{\phi_D}(\mathbf{x}^{(i)} | \mathbf{z}_0, f_\theta) q_{\phi_E}(\mathbf{z}_0 | \mathbf{x}^{(i)}) q_{\phi_\gamma}(\theta | \mathbf{x}^{(i)}) \quad (4)$$

Sampling the transition function f_θ : In contrast to a typical Neural ODEs, we do not tie f_θ to a specific parameter

$\theta \in \Theta$, where Θ is the space of parameters for f_θ . Instead, we model θ as a random variable that conditionally depends on \mathbf{x}_0 . Since θ consists of all parameters in f_θ and therefore is high dimensional, we choose an additional low-dimensional embedding $\gamma \in \Gamma$ to map to Θ with mapping function η such that $\theta = \eta(\gamma)$.

Now, analogous to VAE, we model $q_{\phi_\gamma}(\gamma|\mathbf{x})$ as a Gaussian distribution and learn its parameters, i.e., $(\mu_\gamma, \Sigma_\gamma)$, by training an encoder E_γ . The encoder, E_γ essentially learns to map an observed data $\mathbf{x} = (\mathbf{x}_0, \dots, \mathbf{x}_{T-1})$ (at all T time points) to $(\mu_\gamma, \Sigma_\gamma)$:

$$(\mu_\gamma, \Sigma_\gamma) = E_\gamma(\mathbf{x}) \quad (5)$$

Remark: We use continuous activation functions in f_θ . So, any instantiation of the NN is continuous. Peano existence theorem guarantees the existence of at least one solution to the above ODE locally.

We have now collected the components to (a) sample from $q(\gamma|\mathbf{x})$ and (b) map the embedding γ to the NN parameter θ by learning η . This gives us a sampler to sample f_θ to generate a solution of the corresponding Neural ODE.

Estimate initial condition \mathbf{z}_0 with a Data Encoder $E_{\mathbf{z}_0}$: Similar to the process of learning the latent representation of the transition functions, we learn the distribution of initial values \mathbf{z}_0 as $q_{\phi_E}(\mathbf{z}_0|\mathbf{x}) = \mathcal{N}(\mu_{\mathbf{z}_0}, \Sigma_{\mathbf{z}_0})$, by training an encoder $E_{\mathbf{z}_0}$ to map observed data $\mathbf{x} = (\mathbf{x}_0, \dots, \mathbf{x}_{T-1})$ (at all T time points) to the latent space of \mathcal{Z} whose samples are denoted by \mathbf{z}_t via parameters $(\mu_{\mathbf{z}_t}, \Sigma_{\mathbf{z}_t})$:

$$(\mu_{\mathbf{z}_0}, \Sigma_{\mathbf{z}_0}) = E_{\mathbf{z}_0}(\mathbf{x}) \quad (6)$$

Now, with the initial point, \mathbf{z}_0 and transition function $f(\mathbf{z}_t, t)$ in hand, the remaining step is to map \mathbf{z}_t to the corresponding \mathbf{x}_t in the original data space.

Mapping \mathbf{z} to \mathbf{x} via decoder D : Given the initial value \mathbf{z}_0 and transition function $f(\mathbf{z}_t, t)$, we can use existing ODE solvers to compute \mathbf{z}_t . Once we obtain \mathbf{z}_t using a non-linear function D , we recover the corresponding output \mathbf{x}_t , at time t . We model the output of the process \mathbf{x}_t as a non-linear transformation of the latent measure of progression \mathbf{z}_t as:

$$\mathbf{x}_t = D(\mathbf{z}_t) + \epsilon_t, \quad (7)$$

where ϵ_t is measurement error at each time point. This idea has been variously used in the literature (Pierson et al. 2019; Hyun et al. 2016; Whitaker et al. 2017).

The final model: Combining (5), (6), and (7) we get our Functional ODE model in (8), see Fig. 1.

$$\begin{cases} \mathbf{z}_0 \sim \mathcal{N}(\mu_{\mathbf{z}_0}, \Sigma_{\mathbf{z}_0}), \text{ where } \mu_{\mathbf{z}_0}, \Sigma_{\mathbf{z}_0} = E_{\mathbf{z}_0}(\mathbf{x}) \\ \gamma \sim \mathcal{N}(\mu_\gamma, \Sigma_\gamma), \text{ where } \mu_\gamma, \Sigma_\gamma = E_\gamma(\mathbf{x}) \\ \theta = \eta(\gamma) \mapsto f_\theta \\ \dot{\mathbf{z}}_t = f_\theta(\mathbf{z}_t, t) \\ \mathbf{x}_t = D(\mathbf{z}_t) + \epsilon_t \end{cases} \quad (8)$$

Summary. In contrast to Neural ODE and its variants, for a data \mathbf{x} , we not only use the encoder $E_{\mathbf{z}_0}$ to map the observed data \mathbf{x} to parameters of the distribution of ODE initialization \mathbf{z}_0 , but we also utilize \mathbf{x} and E_γ to sample from function (or embedding) space of NN, characterizing trajectories. Given samples \mathbf{z}_0 and γ (and thus corresponding θ of $f_\theta(\mathbf{z}_t, t)$), the

\mathbf{z}_t are computed as a solution to corresponding ODE, and D is used to map \mathbf{z}_t to \mathbf{x}_t in the original space. Fig. 1 shows an overview. We now show how we can derive ELBO-like likelihood bounds used to train the model in (8).

3.2 ELBO for Functional ODE

The training scheme seeks to learn (a) a distribution of \mathbf{z}_0 , (b) a distribution of γ , which is used to get the corresponding θ by learning (c) a mapping function η , represented by NN. At a high level, our approach is to infer the subspace of the function space, samples from which describe the trajectories, f_θ , of the observed temporal process $\{\mathbf{x}_t\}$. We want to learn two components: an underlying simpler distribution for γ , i.e., $q_{\phi_\gamma}(\gamma|\mathbf{x})$, and mapping η , which maps γ to parameters θ , in-turn defining a sample, f_θ , from the function/embedding space of NNs. A common strategy to learn the underlying distributions, $q_{\phi_\gamma}(\gamma|\mathbf{x})$ and $q_{\phi_E}(\mathbf{z}_0|\mathbf{x})$, is to use a VAE (Chen et al. 2016). It is known that in such probabilistic models, one wants to optimize the likelihood of data \mathbf{x} , but computing this likelihood $p(\mathbf{x})$ is usually intractable. Thus, we use a lower bound as described next.

Let $p(\mathbf{z}_0, \gamma)$ be the joint prior distribution, $q(\mathbf{z}_0, \gamma)$ be an approximate joint posterior. Let $p(\mathbf{x} | \mathbf{z}_0, \gamma)$ be the likelihood of reconstruction, where $\mathbf{x} = (\mathbf{x}_0, \dots, \mathbf{x}_{T-1})$ is a function of the latent representation $\{\mathbf{z}_t\}$. Note that we have two sources of randomness: initial value of the latent trajectory \mathbf{z}_0 , and a latent representation, γ , of a sample from function space of NNs. Using the marginalization property of probabilities, we can write the log likelihood of the data as $\log p(\mathbf{x}) = \log \int p(\mathbf{x}, \mathbf{z}_0, \gamma) d(\mathbf{z}_0, \gamma)$, here $d(\cdot, \cdot)$ is the measure for integral. Using concepts from §2, we can derive a lower bound for the $p(\mathbf{x})$ of our Functional NODE model as:

$$\log p(\mathbf{x}) = \log \int p(\mathbf{x} | \mathbf{z}_0, \gamma) p(\mathbf{z}_0, \gamma) \frac{q(\mathbf{z}_0, \gamma)}{q(\mathbf{z}_0, \gamma)} d(\mathbf{z}_0, \gamma) \quad (9)$$

$$= \log \mathbb{E}_{q(\mathbf{z}_0, \gamma)} \left(p(\mathbf{x} | \mathbf{z}_0, \gamma) \cdot \frac{p(\mathbf{z}_0, \gamma)}{q(\mathbf{z}_0, \gamma)} \right) \geq \mathbb{E}_{q(\mathbf{z}_0, \gamma)} \log p(\mathbf{x} | \mathbf{z}_0, \gamma) - KL(q(\mathbf{z}_0, \gamma) \| p(\mathbf{z}_0, \gamma)), \quad (10)$$

where (9) follows from the definition of joint distribution and using Jensen's inequality.

Next, we define $q(\mathbf{z}_0, \gamma)$ and $p(\mathbf{z}_0, \gamma)$, which is needed to optimize the above lower bound (ELBO).

Choice of $q(\mathbf{z}_0, \gamma)$: Recall that we identify the trajectory as a product of initial value (distribution $q_{\phi_E}(\mathbf{z}_0|\mathbf{x})$) and transition function (distribution $q_{\phi_\gamma}(\gamma|\mathbf{x})$). Thus, we want to find disentangled distribution of \mathbf{z}_0 and γ . This leads to a form where $q(\mathbf{z}_0, \gamma) = q_{\phi_E}(\mathbf{z}_0|\mathbf{x})q_{\phi_\gamma}(\gamma|\mathbf{x})$. Different choices are available to define $q_{\phi_E}(\mathbf{z}_0|\mathbf{x})$ and $q_{\phi_\gamma}(\gamma|\mathbf{x})$ and priors $p(\mathbf{z}_0)$ and $p(\gamma)$, e.g., Horseshoe (Carvalho, Polson, and Scott 2009), spike-and-slab with Laplacian spike (Deng et al. 2019) or Dirac spike (Bai, Song, and Cheng 2020); For our experiments, modeling $q_{\phi_E}(\mathbf{z}_0|\mathbf{x})$, $q_{\phi_\gamma}(\gamma|\mathbf{x})$ and $p(\mathbf{z}_0)$, $p(\gamma)$ as a Gaussian distribution leads to good performance (reconstruction and sample diversity). Other distributions will nonetheless be useful for other real-world time-series datasets.

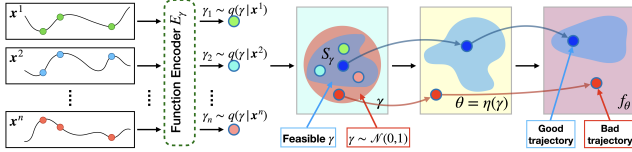


Figure 3: The direct sampling of γ from $N(0, 1)$ results in a bad reconstruction of trajectories. However, given the samples from the learned approximate posterior distribution $q(\gamma|\mathbf{x}^i)$, we can fit a better distribution on top of these samples, referred as S_γ , to generate proper trajectories. The fitting is happened after we train our model.

Training: With all pieces in hand, we summarize the training of functional NODE (FNODE),

Given the observation of temporal process, \mathbf{x} :

1. Use encoder $E_{z_0} : \mathbf{x} = \{\mathbf{x}_t\} \mapsto q_0$ and further sample initial point, z_0 from q_0 .
2. Use encoder $E_\gamma : \mathbf{x} = \{\mathbf{x}_t\} \rightarrow q_\gamma$, and sample latent representation of transition function, γ from q_γ .
3. Use mapping η to map γ to define weights of the NN f_θ and hence characterize $f(z_t, t)$.
4. Use decoder D , fit the FNODE model, by minimizing the loss in (10)

The output from this phase is the latent representation of both components (a) initial value z_0 and (b) transition function $f(z_t, t)$, which allows us to sample temporal processes as in common VAE settings.

Note that if the trajectories are the same for all training samples, then η might collapse to a degenerate distribution due to the singularity. To avoid collapse, we use KL weight annealing (from 0 to 1), (Huang et al. 2018).

Correcting posterior inaccuracies:

While the variational setup is effective in deriving and optimizing for the maximum likelihood, prior results (Kingma et al. 2016) have observed that the Gaussian assumption on the prior $p(z_0, \gamma)$ can often be too restrictive. This results in discrepancies between the prior $p(z_0, \gamma)$ and marginalized approximate posterior $q(z_0, \gamma)$.

To remedy this situation, using more flexible and sometimes hierarchical priors for VAE training (Kingma et al. 2016; Vahdat and Kautz 2020) is useful. However, this leads to additional complexity for optimization since the computation of KL divergence $KL(q(z_0, \gamma) | p(z_0, \gamma))$ can be non-trivial for non-Gaussian priors. Instead, inspired by Ghosh et al. (2020), we empirically found that fitting a Gaussian Mixture Model (GMM) on the learned embeddings z_0, γ in an ex-post manner accounts for the multimodal nature of the data and leads to drastic improvement in sample quality. Since the GMM is learned independently after VAE training on the low-dimensional embeddings, the additional computational complexity is negligible. We refer to this GMM model as S_γ in the sequel.

Implementation: For each sample x^j from the training data, we encode parameters $(\mu_\gamma^j, \Sigma_\gamma^j)$ and draw n_γ independent samples of $\gamma^j \sim N(\mu_\gamma^j, \Sigma_\gamma^j)$. Thus, given N training

samples, we obtain $N \times n_\gamma$ samples of γ , using which a GMM is learned. The motivation for fitting a GMM on samples of $N(\mu_\gamma^j, \Sigma_\gamma^j)$ instead of simply the means μ_γ^j is to also account for the variances Σ_γ^j – the target distribution to approximate is $q(\gamma)$ rather than $q(\mu_\gamma)$. More details on fitting the GMM and selecting the number of components is in the supplement.

3.3 Statistical inference

Given a learned S_γ we can perform different kinds of statistical inference.

Sample generation: Given an initial value z_0 , obtained by encoding some \mathbf{x}^i with E_{z_0} :

1. To sample new trajectories, we can directly sample from S_γ .
2. To sample trajectories described by an example \mathbf{x}^j , we can derive γ_j corresponding to \mathbf{x}^j through the encoder E_γ , and use it to generate a new trajectory from the given z_0 , but which emulates the behavior of \mathbf{x}^j .
3. Relevant to example \mathbf{x}^j , we can also sample $\gamma' \in S_\gamma$, s.t. $|\gamma' - \gamma_j| \leq \delta$. Then, varying a value δ , we can generate new trajectories closer or farther from example \mathbf{x}^j .

Uncertainty estimation: At test time for the given observed temporal process \mathbf{x}^j , we are able to sample trajectories from the learned approximate posterior distribution $q_{\phi_\gamma}(\gamma|\mathbf{x}^j)$ and compute 95% credible intervals (similar to confidence intervals but from a Bayesian perspective), posterior mean and variance. These summary statistics can express the uncertainty regarding temporal trajectories.

Out-of-Distribution (OOD) detection: OOD detection on trajectories is one potential application. In such a setting, outliers are defined by trajectories that have low-probability in the data-generating distribution, and thus unlikely to appear in the dataset.

For conventional temporal models, performing OOD detection is particularly challenging because we must integrate the conditional probabilities $p(x_t|x_{[0,t]})$ over the entire time span $t \in [0, T]$. However, since our method treats trajectories simply as embedded functional instances on which a statistical model is learned directly, there is no need to integrate over the trajectory in order to perform likelihood estimation or statistical testing, which greatly simplifies the formulation.

Advantages: Assuming that the initial condition is fixed for a NODE, there is no variation in the trajectory – so, there is no distribution to setup a statistical test. But in our case, statistical inference is still possible via sampling. Compared to BNNs, via sampling γ , we use a valid likelihood test based on GMM fitted to sampled γ 's. Doing this with BNNs (assuming training succeeds) would either need comparisons of actual trajectories or a test on the posteriors of the entire network's weights.

4 Related work

Bayesian models. While our formulation is different from Neural ODEs (where only the initial condition of the ODE

varies), there are also distinct differences from Bayesian versions of NODE (Yildiz, Heinonen, and Lahdesmaki 2019), where f is parameterized by a Bayesian Neural Network. In general, Bayesian Neural Networks (BNN) (Goan and Fookes 2020) are not considered generative models, like VAE or GAN (Goodfellow et al. 2014). While VAE-based models, as in our work, seek to learn a latent representation of the data (temporal process), the main goal in BNNs is to account for uncertainty in the data, learning a posterior distribution of a *network*, given all the observed data. In contrast to BNN, our work learns an encoding of the temporal process \mathbf{x}^i in its own latent representation $q_{\phi_\gamma}(\gamma|\mathbf{x}^i)$ from which different trajectories are sampled. Conceptually, for each temporal process \mathbf{x}^i , the sampling from latent representations γ_i with distribution $q_{\phi_\gamma}(\gamma|\mathbf{x}^i)$ can be mapped to a BNN form of NODE. However, since the learned latent representation can be considered as a mixture of models, our approach can be thought as a mixture of BNN ODEs. In addition, the latent representation of the trajectory γ allows us to easily perform a likelihood-based test for Out of distribution detection, which is not directly available for Bayesian Network.

Neural ODEs/CDEs. The reader will notice that we sample the entire neural network f_θ , which is otherwise fixed in NODE (Chen et al. 2018) and hence each sample from the space of FNODE is a NODE. This argument can be made more precise. Consider the formulation given in (Kidger et al. 2020). That result (theorem statement in §3.3) notes that any expression of the form $z_t = z_0 + \int_{t_0}^t h_\theta(z_s, X_s) ds$ may be represented exactly by a Neural controlled differential equation (NCDE) of the form as $z_t = z_0 + \int_{t_0}^t f_\theta(z_s) dX_s$. But the converse statement does not hold. In our case, the different γ 's precisely correspond to different X 's i.e., they are functions controlling the evolution of the trajectory. More specifically, γ_1 is the parameterization for a control path (function) X_1 , γ_2 for X_2 and so on. Note that these functions are evaluated along the domain of definition as usual, meaning that $X_1(s) = X_{1,s}$ is the value of the function X_1 at the point s . Therefore, as in (Kidger et al. 2020), our model generalizes NODE in a similar way as NCDE. The distinction between NCDE and FNODE is that the latter deals with modeling a distribution over the control paths (functions) rather than simply one path as in (Kidger et al. 2020).

5 Experiments

We evaluate our model on various temporal datasets, of varying difficulty in the underlying trajectories, representing physical processes, vision data, and human activity. Namely: (1) 3 different datasets from MuJoCo, (2) rotating/moving MNIST, and (3) a longer (100 time steps) real-life data, describing human body pose, NTU-RGBD. Other experiments are in the supplement.

Goals. We evaluate: (a) ability to learn latent representations of the samples of function space, i.e., representation of NN, (b) ability to generate new trajectories, including the trajectories based on examples (c) the ability to perform an Out-of-Distribution analysis for the trajectory and other kinds of statistical inference. We defer details of hardware, neural network architectures, including encoders/decoder and

hyperparameters to the supplement.

Baselines. We compare FNODE with several probabilistic temporal models, namely:

(a) VAE-RNN (Chung et al. 2015), where the full trajectory is encoded in the latent representation; (b) Neural ODE (NODE) (Rubanova, Chen, and Duvenaud 2019), where only initial point of ODE is considered to be stochastic; (c) Bayesian Neural ODE (BNN-NODE)(Yildiz, Heinonen, and Lahdesmaki 2019), where the stochasticity is modeled through initial value z_0 and representing transition function f , using Bayesian version of Neural ODE; (d) Mixed-Effect Neural ODE (Nazarovs et al. 2021), where both components, initial value z_0 and transition function ff , through mixed-effects.

5.1 Variational Sampling of trajectories

We start by showing FNODE’s ability to sample trajectories. Mainly we are interested in validating: (a) for the same initial condition, can our model generate wide variety of trajectories? (b) can our model “transfer” trajectory of an example \mathbf{x}^j to another temporal process \mathbf{x}^i ?

MuJoCo: Data from MuJoCo (Todorov, Erez, and Tassa 2012) provides accurate simulation of articulated structures interacting with their environment to represents simple Newtonian physics. We vary the difficulty of the temporal process, by considering different objects and tasks: humanoid walker, humanoid hopper, and 3 poles cartpole which is a moving along the x-axis cart with rotation of 3 joints, attached to the base. *Sample trajectories:* For each experiment, we randomly generated initial conditions and applied 10 different forces, then we observed 20 time steps. To make visualization easier, we plot every other step. In Figure 4(top), we show trajectories, generated from the same initial value z_0 , but varying samples of the γ (latent representation of the transition function). For all three datasets, we are able to generate diverse and in-distribution trajectories. *Transfer trajectory to other temporal process:* We present a few examples of transferring trajectories in Figure4(Bottom).

In Fig.4, comparing the temporal process in row 1 (from which we derive z_0) and the example in the row 2 (from which we derive γ), there is a large difference in the speed of walker. In row 2 the example needs almost the entire row to fall down from a small height, while the original fall (first row) occurs at a faster pace and from a higher height. As expected, after transfer, the resulting trajectory of our walker (row 4) does not fall down completely, because the pace is slower, derived from row 2, while initial position is at a similar height as in row 1. Similar observations can be made for hopper (2nd set): different speeds of rotation/unbending; and for cartpole: different directions of xx-axis movement (3rd set).

Rotating/Moving MNIST: While MuJoCo provides a wide variety of trajectories, it pertains to the same object. Here, we want to check whether the sampling of trajectories based on an example, works not only within the same class of digits (similar to MuJoCo), but across different styles of Rotating and Moving MNIST.

We model Rotating MNIST by 3 random components: digit (from 0 to 9, any style), random initial rotation, and

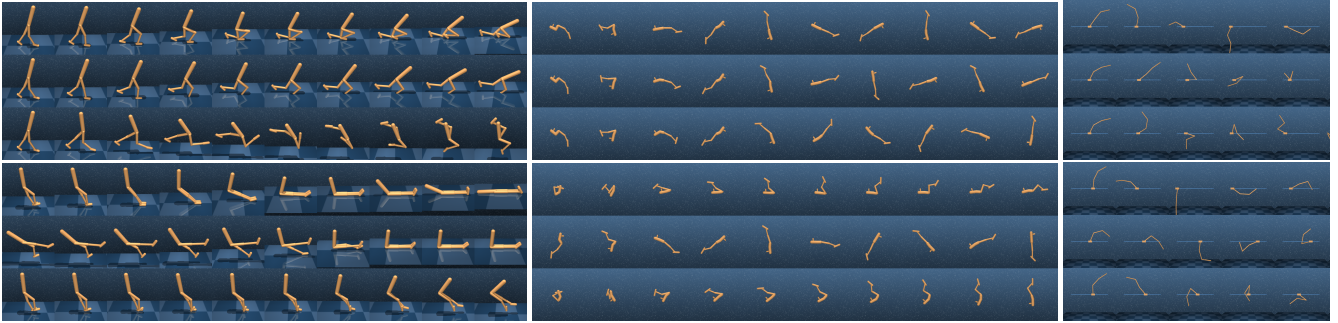
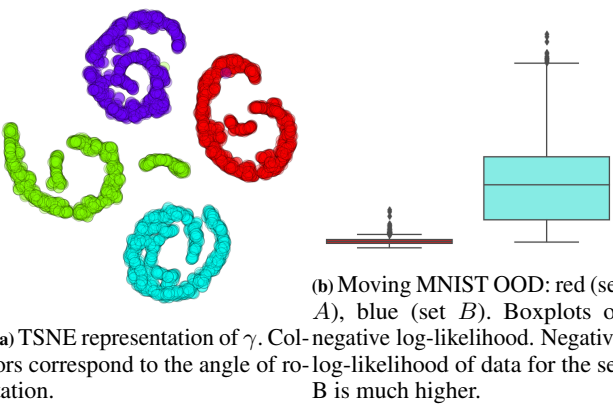


Figure 4: We present visualization of generated trajectories of three different data sets from MuJoCo. From left to right: Walker, Hopper, and 3 poles cartpole. **Top row:** Trajectories are generated by fixing initial condition z_0 and sampling $\gamma \sim S_\gamma$, **Bottom row:** We transfer trajectory by sampling γ from the exemplar, and applying it to z_0 . First row in each block represent original data from which we derive z_0 , second row is an exemplar used to transfer trajectory, and last is sampled/transferred.



Figure 5: Row 1 is a process used to derive z_0 , row 2 is an exemplar, projection of which we would like to transfer, and third row is a result of transfer. Notice how the speed of row 2 transfers to the first row, given an initial condition.



10 different angles of rotation varying from -45° to 45° . For training, we used data observed for 10 time steps. For Moving MNIST we generate 4 random components: digit (from 0 to 9, any style), random initial position and velocity, and 5 different speeds of movement varying from 5 to 50.

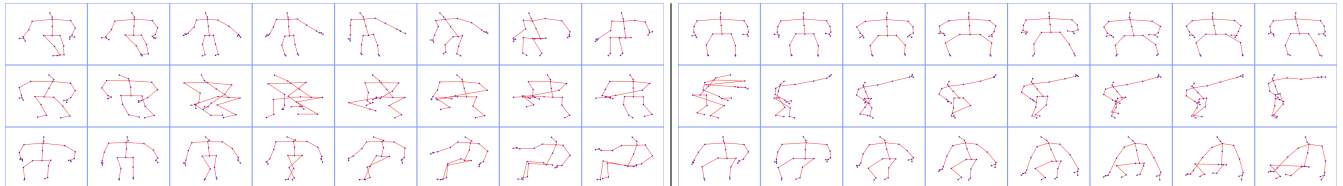
While our goal is variational sampling (and not extrapolating to predict future steps), FNODE provides sensible results for interpolation and extrapolation, compared to other baselines. To this end, for both datasets we generate 20 time-steps. The first 10 time-steps are used as observed to fit the model and learn the distribution of z_0 and γ . The other steps, from 11 to 20, are used to evaluate the ability of our model to extrapolate. In Tab. 1, we provide Mean Squared Error (MSE) for both interpolation and extrapolation. Notice that our method (FNODE) has a smaller interpolation error, compare to other baselines; however, the extrapolation error is higher. This is because we sample both initial value z_0 and representations of the transfer function γ , so we have a wider range of trajectories. We provide plots in supplement. Fig. 5 shows the ability of our model to transfer the trajectory of an exemplar (second row) on the data from which we derived the initial value z_0 (first row). The resultant transferred trajectory is shown in the third row. We see that our model can transfer trajectories across objects of different classes. This implicitly follows from the choice of our model of disentangling trajectory in 2 spaces: space of initial values z_0 and parameterization of the transfer function γ . Notice how smoothly the speed of rotation is transferred to the original data generating a new trajectory. In Figure 6a, we show a TSNE visualization of samples from γ , embedding of transition functions that parameterize trajectories.

Compute/memory efficiency: For batch size 8 (rotation MNIST), our (1) memory need is $3\times$ more than VAE-RNN/NODE/ME-ODE, and $2\times$ more than BNN-NODE. However, for (2) wall-clock time, we need $2\times$ compared to VAE-RNN/NODE, but only $0.75\times$ of ME-ODE/BNN-NODE. Given the benefits of our model, it is a sensible trade-off.

NTU: NTU is a dataset for human actions recognition (Shahroudy et al. 2016). It consists of 126 states with varying number of time-steps. Each state is described by 26 joints

Model	Data									
	Rotating MNIST					Moving MNIST				
	Interpolation	Extrapolation				Interpolation	Extrapolation			
		10%	20%	50%	100%		10%	20%	50%	100%
VAE-RNN	0.0206	0.0865	0.0850	0.0840	0.0831	0.0120	0.0565	0.0587	0.0578	0.0579
NODE	0.0169	0.0903	0.0904	0.0887	0.0863	0.0161	0.0534	0.0566	0.0553	0.0554
BNN-NODE	0.0193	0.0870	0.0870	0.0856	0.0834	0.0208	0.0518	0.0555	0.0537	0.0534
ME-ODE	0.0152	0.0877	0.0875	0.0870	0.0859	0.0193	0.0522	0.0554	0.0552	0.0553
FNODE (Ours)	0.0108	0.0929	0.0932	0.0925	0.0911	0.0100	0.0554	0.0591	0.0590	0.0594

Table 1: Interpolation and Extrapolation MSE, where extrapolation is computed in respect of % of observed steps. Since all methods are probabilistic models, to evaluate MSE we compute the average among generated samples. While interpolation error of our method is lower compared to baselines, the extrapolation error is slightly higher. This happens because our method provides a wide variety of trajectories, so a higher variance.



(a) Initial trajectory and exemplar are actions of sitting, however, on the second row sitting is faster, which results in a fast sitting in the third row

(b) Initial trajectory is a sitting action, while exemplar is hand waving. This results in a novel motion, that in the third row, the person sits but with extended hands.

Figure 7: Represent two different samples of transferring trajectory. First row is a process used to derive z_0 , second row is an exemplar, projection of which we would like to transfer, and third row is a result of transfer. Notice how with the exemplar we can ‘teach’ another object to do similar things.

in 3D coordinates, which are captured using Kinect v2. We select data from 10 states, spanning 100+ time steps. To deal with the longer time series data in the NTU data, we use signature transforms (Morrill et al. 2021). We compute signature transform on the segments of 10 steps with signature depth of 5 (see (Morrill et al. 2021)). We show that despite using the summaries, we are still able to perform satisfactory generation of new trajectories in the observed space. In Fig. 7, we show a 2D projection of human activity, generated by our model. Fig. 7b shows an interesting trajectory, where the model learns from the exemplar to extend the hand, and incorporates this with the sitting action.

5.2 Statistical inference

We show that given a learned distribution of γ , we are able to perform an out-of-distribution analysis, to detect trajectories unfamiliar (or anomalous) for our learned model.

Moving MNIST: We create a dataset A by sampling different MNIST digits, random initial position in the frame and direction and traveling at a given speed. We train our model to learn the embedding of the transition function, γ . Then, we generate additional data traveling at a different velocity (call it B), resulting in a different set of trajectories. We conduct OOD analysis, following the description in Sec.3.3. In Fig. 6b boxplots of negative log-likelihood show a significant difference between groups. Clearly, implicit representation of trajectories using our method is beneficial for OOD.

NTU: We carry out a similar experiment on the NTU dataset. However, here, we increase the number of unknown

Classes of Human Actions	Set A						Set B	
	6	8	9	23	27	36	43	all
Proportion of outliers	0.06	0.07	0.06	0.03	0.05	0.02	0.06	> 0.97

Table 2: Proportion detected as outliers per class in: train set A (in-distribution) and test set B (OOD).

states in the set B . The observed set A , used to train the model, contains information on only about 6 randomly selected classes of human activity. For the testing set B , we use the trajectories from 53 unobserved classes and perform the OOD testing as before. Due to a large number of states, instead of plotting 59 boxplots for negative log-likelihoods, we provide a table with the ratio of points per class, which is defined as an outlier for set A , Table 2. We can see that almost 100% of samples from a set B , not in the training set A , are identified as outliers.

6 Conclusions

We studied mechanisms enabling generation of new trajectories of temporal processes based on variational sampling. Experiments on several real/synthetic datasets show that the sampling procedure is effective in sampling new trajectories and in other statistical inference tasks such as OOD detection, topics that have remained underexplored in the generative modeling literature for temporal data. We note that very high dimensional sequences with complicated temporal dynamics remain out of reach at this time.

A Limitations

Several challenges or limitations in our formulation should be noted. First, since we parameterize f_θ through the computation of both γ and $\eta(\gamma)$, it results in a larger computation graph for backpropagation than a standard NN with parameters as weights. This limitation requires a more careful architectural choice for f_θ . Further, although using a Gaussian Mixture Model S_γ significantly improves the performance of the data decoder to reconstruct unseen trajectories, yet we encounter cases where the performance is not comparable to those from a VAE/GAN for a single frame.

B Societal impacts:

Efficient probabilistic generative models for temporal trajectories, which can be used for uncertainty estimation and other statistical inference tasks such as out of distribution testing, is by and large, a positive development from the standpoint of trustworthy AI models.

C Hardware specifications and architecture of networks

All experiments were executed on NVIDIA - 2080ti, and detailed code will be provided in the github repository later (currently it is attached).

Neural Differential Equations: In any of the implementation we used Runge-Kutta 4 method with ode step size 0.1. To model the equation $\dot{z}_t = f(z_t, t)$, we consider latent representation z_t to be in 1 dimension with p channels. Recall that we learn initial value z_0 from the data directly, and thus we are required to apply encoder.

Encoder E_{z_0} : For the z_0 encoder we use a known and established ode-rnn encoder (Rubanova, Chen, and Duvenaud 2019). For the datasets, like Moving/Rotation MNIST and NTU in addition to ode-rnn encoder we apply a pre-encoder. The main purpose of pre-encoder is to map input in 1 dimensional data with k channels. Which is later used by E_{z_0} to map into p channels.

For **Moving/Rotation MNIST** we use ResNet-18 pre-encoder, with following number of channels (8, 16, 32, 64) for an Encoder.

For **NTU**, the used data consist of 100 time steps with 26 different sensors, and each sensor is with 3d coordinates. As we mentioned in the main paper, we apply the signature transforms. Given the sample with 100 time steps, we split it in chunks of 10, and apply signature transform of depth 5 for each chunk. This results in 10 chunks total with 363 channels (formula: $3 + 3^2 + \dots + 3^5$). As a result of signature transformation we obtain 10 time steps for 86 sensors and 363 channels each. We then apply several FC layers to change number of channels, then we collapse 26 sensors with resulted channels and convert it to k channels, as mentioned above.

```
nn.Sequential(
    nn.Linear(363, 128), nn.ReLU(),
    nn.Linear(128, 256), nn.ReLU(),
    nn.Flatten(2),
```

```
nn.Linear(last_dim * 256, 128),
nn.ReLU(),
nn.Linear(128, output_dim))
```

Encoder E_γ : This is an important part of our modelling, which given temporal observations with T time steps, $x = (x_1, \dots, x_T)$, encodes the information about trajectory into latent representation γ . For this we tried a lot of different encoders, including: **(a)** fully connected, **(b)** neural-ode, **(c)** dilated CNN-1d, **(d)** LSTM, **(e)** RNN, and **(f)** Time Series Transformer. To our surprise the fully connected network performed the best in respect of learning trajectory and training time. The second place was Time Series Transformer.

Projection $\eta : \gamma \implies \theta$: For the projection network η we use a fully connected network, with Tanh() activation function between layers, and after the last layer. Because η eventually returns us weights of a neural network θ , which cannot be extremely big, it was necessary for us not only apply Tanh() as a last layer, but also introduce another single-value parameter λ_θ , which is used to scale $\theta = \lambda_\theta \tanh(F(\gamma))$. We noticed a significant boost in performance once we introduced a tanh on the last layer and a learned scalar λ_θ , compare to weights being completely unbounded.

NN parameterization of transition function f : The previously described weights θ , are the weights of NN, which parameterize f in $\dot{z}_t = f(z_t, t)$. For all experiments we used f as a fully connected network with 3 layers with 100 hidden units each layer and tanh activation function between layers. While the size of this network might look small, empirically it has enough power to model the changes in latent space over time.

Computation aspects of optimization: (This paragraph represents an implementation in the PyTorch, however, it is similar for other popular choices like Tensorflow.) Since we model weight of the NN f , rather than consider them as parameters, we cannot use a standard implementation of layers in PyTorch, like ‘nn.Linear()’. Instead, we create a class of functional networks, where each layer is presented by an operation, like nn.functional.linear. The class is initialized by copying the structure of the provided network, but replacing layers with nn.functional correspondence. The forward function of the class accepts input x and weights θ . Then θ is sliced to fit the size of the current layer and layers is applied to x . As we mentioned in the Limitations of the main paper, this results in a larger than usual computation graph, and requires a more careful architectural choice for f .

Decoder D_x : For the Moving/Rotation MNIST, similar to Encoder E_{z_0} , we use ResNet-18 decoder, but with (32, 16, 8, 8) channels. For other data sets we mainly use fully connected neural networks.

D Selecting GMM

One of the components of our work is to utilize Gaussian Mixture Model (GMM) on top of samples γ from the learned posterior distributions $q_{\phi_\gamma}(\gamma | \mathbf{x}^i)$. The architecture of GMM is based on 2 key factors: number of components and covariance type. To select the best GMM model, which is later used

for sampling from posterior distribution, we range number of components from 10 to 200, with a step 10, and consider 4 different types of covariance matrix provided in python machine learning package “sklearn”: “spherical”, “tied”, “diag”, “full”. Among all these models we select the one with lowest BIC score as the best.

E Experiments

We start the experiment section showcasing a comprehensive analysis of a synthetic panel data set, which conceptually represents observations of multiple individuals over time. Our aim is to showcase the effectiveness of our framework in learning meaningful representations of the transition function f of temporal trajectories.

E.1 Complete analysis of a synthetic panel data

To demonstrate the ability of our framework to learn meaningful representation of the transition function f of temporal trajectories, we consider a synthetic panel data, which is represented in the form:

$$\begin{cases} x_t^{(i)} = A^{(i)} \cdot \sin(\psi_t^{(i)}) + \varepsilon^{(i)} \\ \frac{d\psi_t^{(i)}}{dt} = 2\pi \\ \varepsilon^{(i)} \sim N(0, 10^{-3}) \end{cases} \quad (11)$$

In this representation, $x_t^{(i)}$ conceptually might represent the i patient’s observation at time t , for example, it can describe amyloid accumulation in the region of the brain (Bettauer et al. 2022). The derivative of $x_t^{(i)}$ with respect to t represents the rate of change of $x_t^{(i)}$ with respect to time. The amplitude of changes $A^{(i)}$ is defined per group i , e.g. patient, and can vary among groups. While $x_t^{(i)}$ can be a multi-dimensional vector, without loss of generality we consider $x_t^{(i)}$ to be a one dimensional. Namely, for each group i at time step t , $x_t^{(i)}$ is 1 dimensional vector.

For this set of experiments, we generate 10,000 examples with 10 unique values of $A^{(i)} \sim \text{Unif}(0, 10)$. In addition to make data more complicated in separation, and check that our framework is capable to capture the difference in transition functions $f^{(i)}$, rather than underlying $z_0^{(i)}$, we use the same initial condition $x_0^{(i)} = 0, \forall i$. We generate data for $t \in [0, 1.5]$, and randomly sample 10 time points for each individual data entry as observed data.

Learning a meaningful representation of transition function. Studying the form of equation (11), it is clear that samples of $x_t^{(i)}$ are separated corresponding to different values of $A^{(i)}$. To illustrate the ability of our model to learn meaningful representation of transition functions $f^{(i)}$, we plot T-SNE representation of learned by our framework $\gamma^{(i)}$, Figure 8. While there is some overlap between classes of derived *gammas* corresponding to different values of amplitude A , there is a clear separation as one would expect by observing equation (11). A good separation between encoded values γ of temporal trajectories allows us to perform statistical inference, including sampling, which we are going to talk about next.

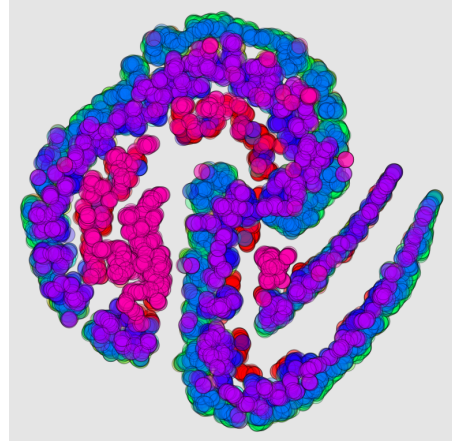


Figure 8: T-SNE representation of learned by our framework $\gamma^{(i)}$, which correspond to embedding of transition function $f^{(i)}$ of corresponding data trajectories. Each color corresponds to a different value of amplitude $A^{(i)}$.

Variational sampling of temporal trajectories. Recall, we described how we can correct posterior inaccuracies of learned approximate posterior distribution of $\gamma^{(i)}$, which allows us to perform variational sampling of high quality. Namely, for each sample x^j from the training data, we encode parameters $(\mu_\gamma^j, \Sigma_\gamma^j)$ and draw n_γ independent samples of $\gamma^j \sim N(\mu_\gamma^j, \Sigma_\gamma^j)$. Thus, given N training samples, we obtain $N \times n_\gamma$ samples of γ , using which a GMM is learned.

Given a learned GMM, we are able to sample temporal trajectories corresponding to data $x^{(i)}$, which is presented in Figure 9. In addition to observed values used for training the model (crosses on the image), we represent the 95% credible interval (red region) and a posterior mean (red dashed line), which are derived through sampling $\gamma^{(i)}$ from learned GMM and passing it through decoder, to obtain new values $\hat{x}^{(i)}$. As we can see that all observed values lie inside the credible interval, which indicate a simple check of our model’s capability to generate variational samples of temporal trajectories. Next, we are going to discuss more of a statistical inference, and demonstrate the usability of our framework to detect trajectories outside the distribution.

Out-of-Distribution (OOD) detection. To evaluate the ability of our model to detect OOD trajectories, we introduce another set of trajectories, defined as:

$$\begin{cases} x_t^{B,(i)} = \sin(\psi_t^{(i)}) + \varepsilon^{(i)} \\ \frac{d\psi_t^{(i)}}{dt} = 2\pi \cdot B^{(i)} \\ \varepsilon^{(i)} \sim N(0, 10^{-3}) \end{cases} \quad (12)$$

Similar to the previous setup, $x_t^{B,(i)}$ conceptually might represent the i patient’s observation at time t , but belongs to the group with an underlying biological risk factor, which effects the development of the temporal process $x_t^{B,(i)}$. In this case the frequency coefficient $B^{(i)}$ is defined per group i , e.g. patient, and can vary among groups.

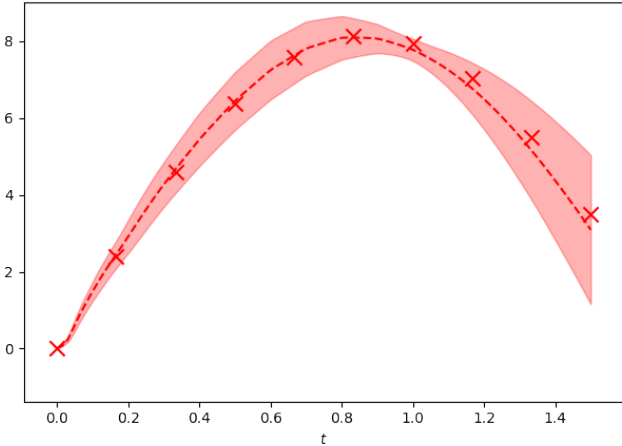


Figure 9: We demonstrate the variational sampling of temporal trajectories, given the 10 samples of observed data (x) used to train the model to derive representation of transition function. Red region is 95% credible interval and dashed line corresponds to the posterior mean.

We generate 10,000 examples with 10 unique values of $B^{(i)} \sim \text{Unif}(0, 10)$, with the same initial condition $x_0^{B, (i)} = 0, \forall i$. We generate data for $t \in [0, 1.5]$, and randomly sample 10 time points for each individual data entry as observed data.

Recall, we describe the ability of our model to conduct OOD. Given a set of observed data $x^{(i)}$, we train our model to learn the approximate posterior distribution (and corresponding GMM) of $\gamma^{(i)}$ – the latent representation of transition functions corresponding to $x^{(i)}$. Then, given a trained model, we embed newly observed trajectories $x^{B, (i)}$ to the $\gamma^{B, (i)}$ and conduct the likelihood outlier test to understand whether $\gamma^{B, (i)}$ belongs to the learned GMM – distribution of $\gamma^{(i)}$. In Figure 10 we present two findings: on the left side we have a T-SNE representation of embedding of trajectories and on the right, the boxplot of negative log-likelihood for corresponding samples. As we can see, the negative log-likelihood of data for the set B is much higher than for a training set, which clearly indicates the outlier nature of set B.

In the following subsection we provide an in-depth exploration of variational sampling of trajectories and statistical inference techniques, which is performed on more complex computer vision data sets, demonstrating the versatility of our framework.

E.2 Pittsburgh Compound B or PIB data

To show the ability of our model to do a variational sampling of temporal trajectories with limited number of samples, we consider Pittsburgh Compound B data (Betthauser et al. 2022). Data contains 314 records of patients, with each record up to 6 time steps. PIB data provides information about 118 regions of brain scans, patients age at visit and has a property of irregular time series.

In Figure 11 we provide an example of variational sampling of temporal trajectories of one of the 118 brain regions

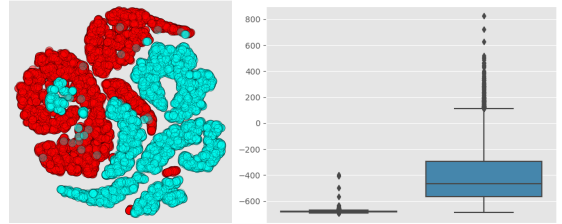


Figure 10: Outlier test: red is set participating in the training, blue is newly observed set B. Noticed the meaningful separation in T-SNE representation of embedding between two distributions. in addition, we provide boxplots of negative log-likelihood for corresponding samples. As we can see, the negative log-likelihood of data for the set B is much higher, then for a training set, which clearly indicates the outlier nature of set B.

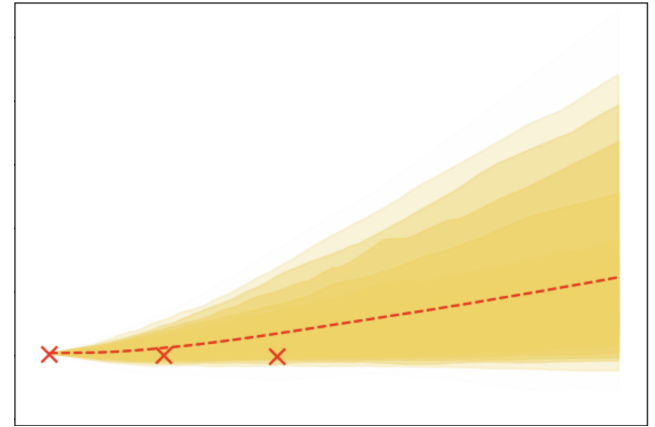


Figure 11: Variational sampling of temporal trajectories of one of the 118 brain regions for 6 time steps, given only 3 time steps observed per patient. Yellow lines are generated trajectories, red dashed line is a posterior average, and red crosses are observed time steps.

for 6 time steps, given only 3 time steps observed per patient.

E.3 Rotating MNIST

In this section we provide additional samples of trajectories. To show the quality of our reconstruction, regardless of MSE values from the table in main paper, in Figure 12 we present the ablation studies of several samples for different baselines.

In addition to comparison to quality of reconstruction, we show the variation of samples derived by sampling different representations of the transition function γ , but preserving the initial value of the latent representation z_0 .

E.4 MuJoCo

Below we provide several samples from our model for different sets of MuJoCo, namely Hopper, Walker and 3-poles cart. Notice how trajectories are different, despite the same initial values.

References

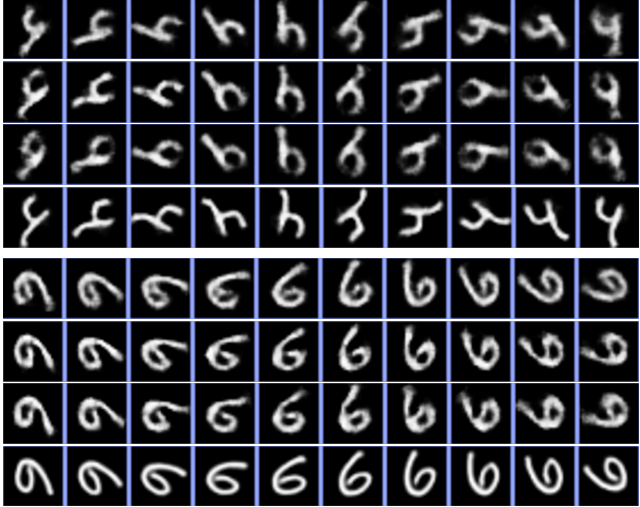


Figure 12: Reconstruction of the same samples, from top to bottom by block: VAE-RNN, NODE, BNN-NODE, FODE (our). Clearly, our model provides the most clear reconstruction.

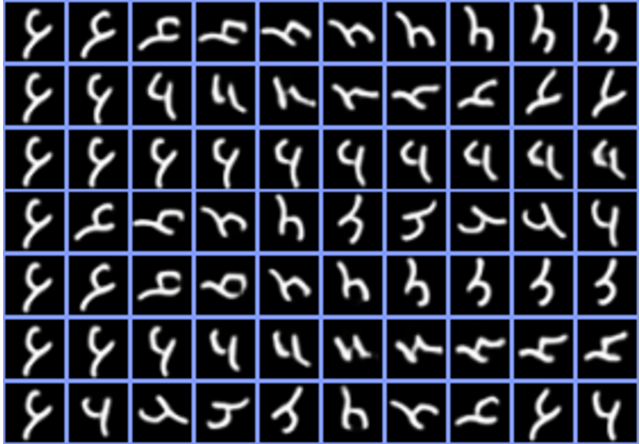
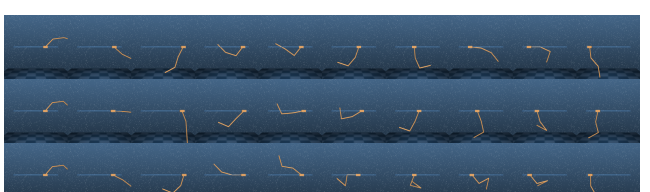
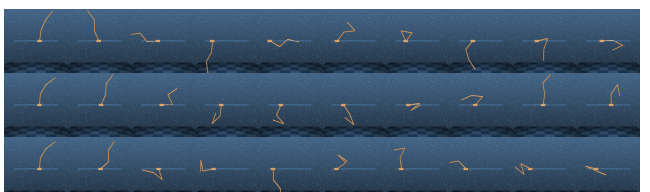
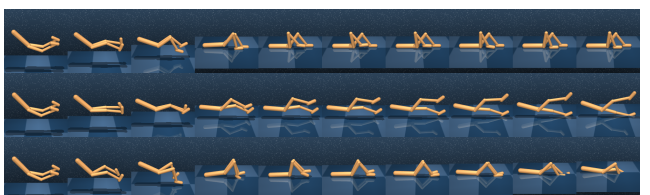
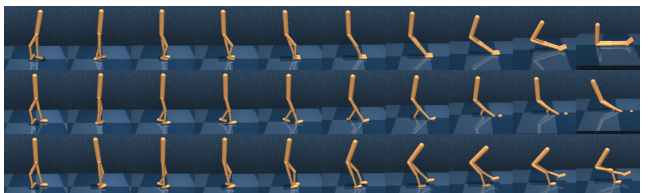
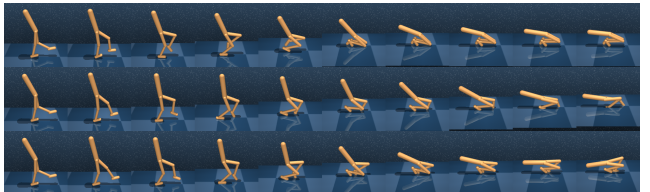
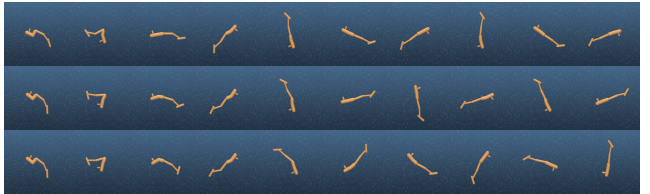
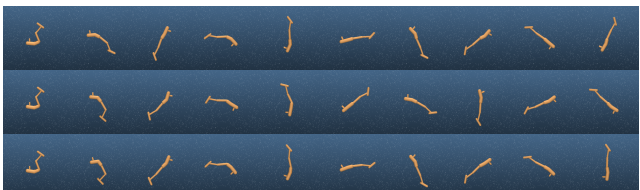


Figure 13: Variation of samples for our model. Notice the difference in the angle of rotation given the same initial value, but varying the representation of transition function γ .



- [1] Bai, J.; Song, Q.; and Cheng, G. 2020. Efficient Variational Inference for Sparse Deep Learning with Theoretical Guarantee. *arXiv preprint arXiv:2011.07439*.
- [2] Betthauser, T. J.; Bilgel, M.; Koscik, R. L.; Jedynak, B. M.; An, Y.; Kellett, K. A.; Moghekar, A.; Jonaitis, E. M.; Stone, C. K.; Engelman, C. D.; et al. 2022. Multi-method investigation of factors influencing amyloid onset and impairment in three cohorts. *Brain*, 145(11): 4065–4079.
- [3] Brunton, S. L.; Noack, B. R.; and Koumoutsakos, P. 2020. Machine learning for fluid mechanics. *Annual Review of Fluid Mechanics*, 52: 477–508.
- [4] Carvalho, C. M.; Polson, N. G.; and Scott, J. G. 2009. Handling sparsity via the horseshoe. In *Artificial Intelligence and Statistics*, 73–80. PMLR.
- [5] Chen, R. T.; Rubanova, Y.; Bettencourt, J.; and Duvenaud, D. K. 2018. Neural ordinary differential equations. *Advances in neural information processing systems*, 31: 6571–6583.
- [6] Chen, X.; Kingma, D. P.; Salimans, T.; Duan, Y.; Dhariwal, P.; Schulman, J.; Sutskever, I.; and Abbeel, P. 2016. Variational lossy autoencoder. *arXiv preprint arXiv:1611.02731*.
- [7] Cho, K.; Van Merriënboer, B.; Gulcehre, C.; Bahdanau, D.; Bougares, F.; Schwenk, H.; and Bengio, Y. 2014. Learning phrase representations using RNN encoder-decoder for statistical machine translation. *arXiv preprint arXiv:1406.1078*.
- [8] Chung, J.; Kastner, K.; Dinh, L.; Goel, K.; Courville, A. C.; and Bengio, Y. 2015. A recurrent latent variable model for sequential data. *Advances in neural information processing systems*, 28.
- [9] Deng, W.; Zhang, X.; Liang, F.; and Lin, G. 2019. An adaptive empirical bayesian method for sparse deep learning. *Advances in neural information processing systems*, 2019: 5563.
- [10] Devlin, J.; Chang, M.-W.; Lee, K.; and Toutanova, K. 2018. Bert: Pre-training of deep bidirectional transformers for language understanding. *arXiv preprint arXiv:1810.04805*.
- [11] Dupont, E.; Kim, H.; Eslami, S.; Rezende, D.; and Rosenbaum, D. 2022. From data to functa: Your data point is a function and you should treat it like one. *arXiv preprint arXiv:2201.12204*.
- [12] Ghosh, P.; Sajjadi, M. S. M.; Vergari, A.; Black, M.; and Scholkopf, B. 2020. From Variational to Deterministic Autoencoders. In *International Conference on Learning Representations*.
- [13] Goan, E.; and Fookes, C. 2020. Bayesian neural networks: An introduction and survey. In *Case Studies in Applied Bayesian Data Science*, 45–87. Springer.
- [14] Goodfellow, I.; Pouget-Abadie, J.; Mirza, M.; Xu, B.; Warde-Farley, D.; Ozair, S.; Courville, A.; and Bengio, Y. 2014. Generative adversarial nets. *Advances in neural information processing systems*, 27.
- [15] Hochreiter, S.; and Schmidhuber, J. 1997. Long short-term memory. *Neural computation*, 9(8): 1735–1780.
- [16] Huang, C.-W.; Tan, S.; Lacoste, A.; and Courville, A. C. 2018. Improving explorability in variational inference with annealed variational objectives. *Advances in Neural Information Processing Systems*, 31.
- [17] Hyun, J. W.; Li, Y.; Huang, C.; Styner, M.; Lin, W.; Zhu, H.; Initiative, A. D. N.; et al. 2016. STGP: Spatio-temporal Gaussian process models for longitudinal neuroimaging data. *Neuroimage*, 134: 550–562.
- [18] Kidger, P.; Morrill, J.; Foster, J.; and Lyons, T. 2020. Neural controlled differential equations for irregular time series. *Advances in Neural Information Processing Systems*, 33: 6696–6707.
- [19] Kingma, D. P.; Salimans, T.; Jozefowicz, R.; Chen, X.; Sutskever, I.; and Welling, M. 2016. Improved Variational Inference with Inverse Autoregressive Flow. In Lee, D.; Sugiyama, M.; Luxburg, U.; Guyon, I.; and Garnett, R., eds., *Advances in Neural Information Processing Systems*, volume 29. Curran Associates, Inc.
- [20] Kingma, D. P.; and Welling, M. 2013. Auto-encoding variational bayes. *arXiv preprint arXiv:1312.6114*.
- [21] Lewis, M.; Liu, Y.; Goyal, N.; Ghazvininejad, M.; Mohamed, A.; Levy, O.; Stoyanov, V.; and Zettlemoyer, L. 2019. Bart: Denoising sequence-to-sequence pre-training for natural language generation, translation, and comprehension. *arXiv preprint arXiv:1910.13461*.
- [22] Lusch, B.; Kutz, J. N.; and Brunton, S. L. 2018. Deep learning for universal linear embeddings of nonlinear dynamics. *Nature communications*, 9(1): 1–10.
- [23] Morrill, J.; Salvi, C.; Kidger, P.; and Foster, J. 2021. Neural rough differential equations for long time series. In *International Conference on Machine Learning*, 7829–7838. PMLR.
- [24] Nazarov, J.; Chakraborty, R.; Tasneeyapant, S.; Ravi, S.; and Singh, V. 2021. A variational approximation for analyzing the dynamics of panel data. In *Uncertainty in Artificial Intelligence*, 107–117. PMLR.
- [25] Nilsson, D.; and Sminchisescu, C. 2018. Semantic video segmentation by gated recurrent flow propagation. In *Proceedings of the IEEE conference on computer vision and pattern recognition*, 6819–6828.
- [26] Pierson, E.; Koh, P. W.; Hashimoto, T.; Koller, D.; Leskovec, J.; Eriksson, N.; and Liang, P. 2019. Inferring multidimensional rates of aging from cross-sectional data. *Proceedings of machine learning research*, 89: 97.
- [27] Radford, A.; Narasimhan, K.; Salimans, T.; and Sutskever, I. 2018. Improving language understanding by generative pre-training.
- [28] Rubanova, Y.; Chen, R. T.; and Duvenaud, D. K. 2019. Latent ordinary differential equations for irregularly-sampled time series. In *Advances in Neural Information Processing Systems*, 5320–5330.
- [29] Rudy, S. H.; Brunton, S. L.; Proctor, J. L.; and Kutz, J. N. 2017. Data-driven discovery of partial differential equations. *Science advances*, 3(4): e1602614.
- [30] Shahroudy, A.; Liu, J.; Ng, T.-T.; and Wang, G. 2016. Ntu rgb+ d: A large scale dataset for 3d human activity analysis. In *Proceedings of the IEEE conference on computer vision and pattern recognition*, 1010–1019.
- [31] Strike, L. T.; Hansell, N. K.; Chuang, K.-H.; Miller, J. L.; de Zubiray, G. I.; Thompson, P. M.; McMahon, K. L.; and Wright, M. J. 2022. The Queensland Twin Adolescent Brain Project, a longitudinal study of adolescent brain development. *bioRxiv*.
- [32] Todorov, E.; Erez, T.; and Tassa, Y. 2012. Mujoco: A physics engine for model-based control. In *2012 IEEE/RSJ International Conference on Intelligent Robots and Systems*, 5026–5033. IEEE.
- [33] Tzen, B.; and Raginsky, M. 2019. Neural stochastic differential equations: Deep latent gaussian models in the diffusion limit. *arXiv preprint arXiv:1905.09883*.
- [34] Vahdat, A.; and Kautz, J. 2020. NVAE: A Deep Hierarchical Variational Autoencoder. In Larochelle, H.; Ranzato, M.; Hadsell, R.; Balcan, M.; and Lin, H., eds., *Advances in Neural Information Processing Systems*, volume 33, 19667–19679. Curran Associates, Inc.

- [35] Whitaker, G. A.; Golightly, A.; Boys, R. J.; Sherlock, C.; et al. 2017. Bayesian inference for diffusion-driven mixed-effects models. *Bayesian Analysis*, 12(2): 435–463.
- [36] Yildiz, C.; Heinonen, M.; and Lahdesmaki, H. 2019. ODE2VAE: Deep generative second order ODEs with Bayesian neural networks. In *Advances in Neural Information Processing Systems*, 13412–13421.